JOURNAL OF AIRCRAFT
Vol. 35, No. 4, July–August 1998

High-Performance Airfoil with Moving Surface Boundary-Layer Control

V. J. Modi,* S. R. Munshi,† and G. Bandyopadhyay‡
University of British Columbia, Vancouver, British Columbia V6T 1Z4, Canada
and
T. Yokomizo§
Kanto Gakuin University, Mutsuura, Kanazawa, Yokohama 236, Japan

All airfoils are known to stall at high angles of attack as a result of flow separation, resulting in a sudden loss of the lift force. To avoid flow separation, it is necessary to introduce some form of boundary-layer control. The present study focuses on the performance of an airfoil with moving surface boundary-layer control (MSBC). Effects of the angles of attack, rate of momentum injection, as well as rotating cylinder surface condition on the surface pressure distribution and aerodynamic coefficients are assessed. A comprehensive study involving wind-tunnel investigation, numerical simulation, and flow visualization clearly demonstrates that the momentum injection through MSBC results in a significant delay in the stall angle (from 10 to 50 deg) and an increase in the lift coefficient by more than 200% at high angles of attack ($\alpha \approx 30$ deg). The results show that a multielement panel method, modeling the flow separation using free vortex lines, predicts the overall aerodynamics of an airfoil with the MSBC quite accurately. The airfoil performance can be improved further by judicious selection of the rotating cylinder surface condition. Among the three different surface roughness conditions studied, the cylinder with axial splines was found to be the most effective.

Introduction

THE next generation of high-performance airplanes demand improved aerodynamics as well as better maneuverability. Research in the area of high-angle-of-attack aerodynamics as applied to single and multielement airfoils continues to receive further attention. The high-α condition can be viewed broadly as an off-design condition where the airplane or any of its components are in a high-lift environment.[1] This high-α region is characterized by small- and large-scale, static, and dynamic flowfield interactions that may include regions of attached flow as well as unorganized separated flow. These interactions are frequently strong enough to affect the global aerodynamics of the airplane.[1] The use of boundary-layer control to increase lift and delay stall of an airfoil is quite well known. Methods such as suction, blowing, vortex generators, turbulence promoters, oscillatory surface flaps, acoustic excitation, oscillatory heating, etc., have been studied at length and applied in practice with a varying degree of success. A vast body of literature accumulated over the years has been reviewed rather effectively.[2–7] Apart from methods such as blowing and suction, a combination of unsteady excitation technique, e.g. a leading-edge flap oscillation, and special wing configurations that provide a comfortable seat to capture lift-producing vortices and room for wave–vortex resonance have been proposed for vortex flow control of an airfoil in the poststall regime.[8] However, the use of a moving wall for boundary-layer control has received relatively less attention. This is indeed surprising because the concept of moving surface boundary-layer control (MSBC) appears quite promising. It has already proved successful in lift augmentation,[9] drag reduction (by as much as 80%) of bluff bodies as well as the suppression of flow-induced vibrations.[10–12] The moving surface is provided by a high-speed rotating cylinder, which replaces the leading edge of the airfoil. This concept has a long and interesting history dating back to more than a century, including contributions by Magnus, Prandtl, Flettner, Favre, Tennant, and others. Modi et al.[9] have reviewed this literature at some length. Successful flight tests have also been performed on the North American Rockwell's OV-10A by NASA Ames Research Center.[13,14] Here the leading edge of the flap was replaced by a high-speed rotating cylinder.

The main objective of the MSBC is to prevent, or at least delay, separation of the boundary layer from the wall. This is accomplished in the following ways: 1) a moving surface retards the growth of the boundary layer by minimizing the relative motion between the surface and the freestream; 2) it injects momentum into the boundary layer; 3) it creates a region of high suction and thereby accelerates the flow in its neighborhood outside of the boundary layer; and 4) it delays separation and interferes with the evolution of the wake.

A rotating cylinder provides additional circulation through the differential jump in the velocity at the upper surface with respect to the lower surface of the cylinder. Vorticity is also generated in the boundary layer around the rotating cylinder. Thus a rotating cylinder can provide considerably higher lift.

One would like to assess the relative merit of the moving surface boundary-layer control with other procedures for boundary-layer control such as suction, blowing, etc. Obviously, to be useful, such a comparison has to be based on well-planned experiments conducted under controlled and comparable conditions; otherwise it can lead to misleading conclusions. Unfortunately, such results permitting rational comparison have not been recorded in the literature. However, it is possible to make a few general observations.

Presented as Paper 96-3445 at the AIAA Atmospheric Flight Mechanics Conference, San Diego, CA, July 29–31, 1996; received April 2, 1997; revision received Oct. 21, 1997; accepted for publication Nov. 15, 1997.

*Professor Emeritus, Department of Mechanical Engineering.
†Postdoctoral Research Fellow, Department of Mechanical Engineering. Member AIAA.
‡Visiting Research Associate, Department of Mechanical Engineering; currently Associate Professor, Department of Aerospace Engineering, Indian Institute of Technology, Kharagpur, India.
§Professor, Department of Mechanical Engineering.

Besides its striking success in increasing the lift of airfoils or reducing the drag of bluff bodies, one of the attractive features of the moving surface boundary-layer control is the negligible amount of power involved in driving the cylinders. Essentially it corresponds to the bearing friction and the torque contributed by the forces on the surface of the cylinder. Note, the cylinders itself can be hollow thus minimizing the inertia effect. Hence, the power required to drive the rotating elements is relatively negligible. Wygnanski and Seifert[15] have reported a significant increase in lift and reduction in drag through steady and oscillatory blowing over a slotted flap.

An experiment to measure the power consumption was performed on the rotating cylinder (diameter = 0.038 m, length = 0.733 m, mass = 2033 g) used in the airfoil model. At the maximum rate of momentum injection (U_C/U = 4, U = 5.9 m/s, N = 12,000 rpm), the power consumed was about 0.22 hp. Most of the energy is expended in overcoming the bearing friction, the contribution resulting from aerodynamic resistance being marginal.

For example, consider the case of boundary-layer control through suction. Calculation of total suction power as applied to a typical airplane (total weight = 4500 kg, wing area = 23 m^2) required anywhere from 15 to 35 hp, depending on the type of system used.[16] In this case C_L was raised from 0.87 to 1.5 and the α_{stall} from 10.5 to 15 deg. The YOV-10A aircraft from North American Rockwell[17] has similar characteristics (total weight $\approx$ 4500 kg, wing area $\approx$ 27 m^2, powerplant = 2 $\times$ 715 hp). The YOV-10A was fitted with rotating cylinder flaps and flight tested to assess its performance.[18] For such an application the estimated power requirements are somewhere below 2% of the engine power.[19] This would amount to 29 hp. The experiments have shown that with MSBC the α_{stall} can be raised from 10 to 48 deg with a maximum C_L of 2.35.[9] Obviously, in this operational range, application of the boundary-layer suction would require considerably more power.

With this as the background, the paper presents results of an extensive study having three phases:

1) Wind-tunnel tests as applied to an airfoil with the MSBC. Effects of the angle of attack, rate of momentum injection U_C/U (U_C = cylinder surface velocity; U = freestream velocity), as well as a rotating cylinder surface condition on the surface pressure distribution and aerodynamic coefficients are assessed in this phase.

2) Next, the system performance is predicted by numerical simulation of a multielement airfoil using a rather simple yet effective surface singularity approach.

3) Finally, a flow visualization study in a closed-circuit water channel using polyvinyl chloride particles as tracers in the presence of slit lighting complements the wind tunnel and numerical investigations. Still photographs as well as video movies were taken.

Wind-Tunnel Investigation

Model and Test Arrangement

A 16%-thick symmetric Joukowsky airfoil with a chord length of 370 mm, fitted with a leading-edge rotating cylinder (diameter 37 mm), spanned the tunnel test section, 0.91 $\times$ 0.68 m, to create an essentially two-dimensional condition (Fig. 1a). The rotating cylinder is driven by a 1/4-hp, variable-speed, ac motor. Forty-two pressure taps, 0.5 mm in diameter, are located at the top and bottom surfaces of the airfoil. The tests were carried out in a low-speed, low-turbulence, closed-circuit wind tunnel, where the airspeed can be varied from 1–50 m/s with a turbulence level less than 0.1%. The pressure distribution was recorded using a sensitive barocel pressure transducer, with a resolution of 6.9 $\times$ 10^{-5} N/m^2, connected to a data acquisition system. The force data were obtained through integration of the pressure results.

The tests were conducted over an extended range of the angle of attack (α = 0–50 deg) with an increment anywhere from 5–10 deg depending on the flowfield of interest. The cylinder rotation speed was varied to give U_C/U in the range of 0–4 with the Reynolds number (based on the chord of the airfoil) of around 1.43 $\times$ 10^5. The measurement of pressure on the surface of the cylinder, rotating typically at 6000–12,000 rpm, presents a challenge. This problem was resolved by keeping the pressure rings, located in a narrow groove, stationary while the cylinder rotated (Fig. 1b).

Rotating cylinders with three different surface conditions are shown in Fig. 1c. The splined cylinder has 10 axially parallel surface grooves. The width and the depth of these grooves is about 15 and 5% of the cylinder diameter, respectively. The rough cylinder has flat surface projections (5% thick, 18% wide, and 55% long—based on cylinder diameter). The longitudinal and circumferential grooves act as tiny vortex generators, and it was anticipated that this would increase effectiveness of the momentum injection.

To provide reference information to facilitate comparison, tests were carried out with the basic airfoil, i.e., original Joukowsky airfoil without rotating cylinder. Detailed pressure distribution plots for three angles of attack (including the stall at α = 18 deg) are presented in Fig 1d. Corresponding variation of C_L with the angle of attack is shown in Fig. 1e. It also shows the effect of modifying the nose geometry through the presence of a rotating cylinder and a gap. As can be expected, the modified airfoil in the absence of rotation has lower $C_{L,max}$ and stalls earlier.

Lift and Drag Characteristics

Variations in the lift coefficient with the angle of attack for smooth, rough, and splined rotating cylinders are presented in Fig. 2. The airfoil with a smooth leading-edge cylinder is the benchmark case (Fig. 2a) and all other results are compared with it. In absence of cylinder rotation (U_C/U = 0), the airfoil stalls at around α = 10–15 deg, depending on the type of rotating cylinder employed. In case of the smooth cylinder (Fig. 2b), as the cylinder rotation speed is increased from U_C/U = 0 to 4, the stall is delayed progressively to higher angles of attack: 15 deg at U_C/U = 1; 25 deg at U_C/U = 2; and 30–35 deg at U_C/U = 3–4. There is a corresponding increase in the lift coefficient (C_L) with α. For a momentum injection rate in the range U_C/U = 3–4, the $C_{L,max}$ of 1.84 for the smooth cylinder represents an increase of around 160%. The corresponding gain with the splined cylinder surface was equally impressive at 210% ($C_{L,max}$ = 2.2). As α is increased beyond 35 deg, C_L decreases, but the stall is very gradual, i.e., it does not fit the nominal definition of a stall, because a rapid loss in lift is avoided. Even for α as high as 50 deg, C_L is about 1.48 (smooth cylinder), which is quite remarkable. The rate of change in C_L with α can be estimated from the slope $dC_L/d\alpha$. There is no significant change in the slope of the lift curve with the smooth rotating cylinder case. However, with the rough and splined rotating cylinders there is a small rise in $dC_L/d\alpha$ with an increase in the momentum injection. Note, there is no additional appreciable benefit in terms of an increase in lift when the momentum injection is raised from U_C/U = 3 to 4. This indicates a practical limit to the beneficial influence of the momentum injection.

Compared to the smooth-surface rotating cylinder, the rough cylinder has inferior performance (Fig. 2b). The maximum C_L is about 1.52 at α = 30 deg, which is lower than that obtained with a smooth cylinder ($C_{L,max}$ = 1.84). The axial grooves on the splined cylinder scoop the incoming fluid, and thereby improve momentum injection in the boundary layer. It is of interest to point out that, as reported by Modi et al.,[20] the splined cylinder proved quite successful in reducing the drag of a tractor-trailer truck configuration. In fact, this served as a motivation to assess the scooping effect of a splined cylinder when applied to an airfoil. In the case of the rough-surface cylinder, the axial splines are supplemented by circumferential grooves (Fig. 2c), which seem to disrupt the effective scooping mech-

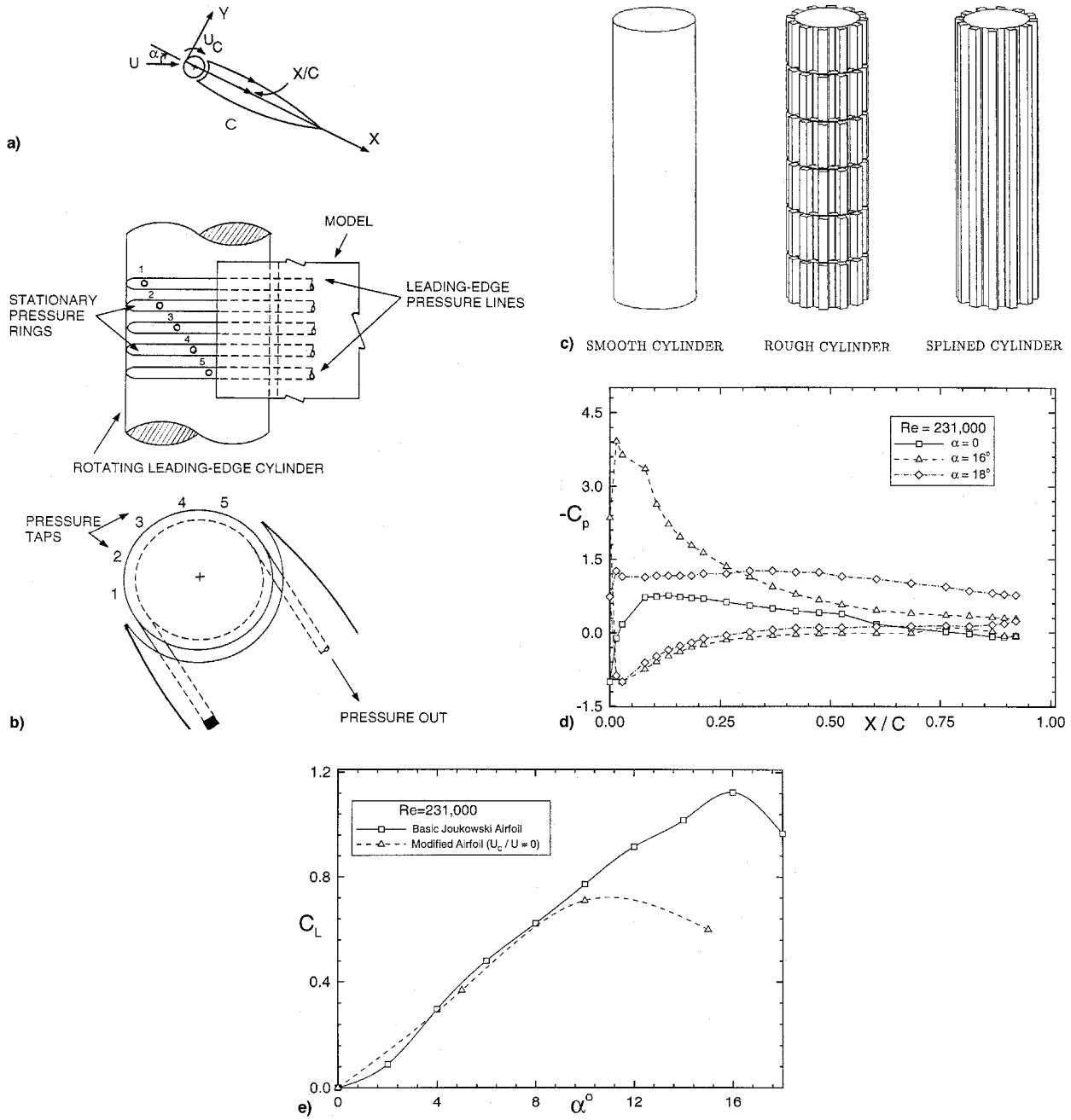

Fig. 1 a) Symmetrical Joukowski airfoil with its nose replaced by a rotating cylindrical element; b) schematic diagram showing details of the pressure taps near the rotating element; c) rotating cylinders, with three different types of surface conditions, used in the test program; d) experimentally obtained pressure distribution for a 16%-thick basic Joukowski airfoil; and e) variation of the lift coefficient with angle of attack for the basic Joukowski airfoil. Results for the modified airfoil at $U_C/U = 0$ are also included to facilitate comparison.

anism. The axial splines extend along the axis of the rotating cylinder from end to end, maintaining a two-dimensional flow. On the other hand, the circumferential grooves interfere with a two-dimensional character of the flow resulting in a deteriorated performance. Turbulence may also affect the situation. Table 1 lists $C_{L,max}$ and stall values for the three different cylinder surface conditions. In Table 2, average values of the slope $dC_L/d\alpha$ are listed. It is apparent that the performance of the spline surface cylinder is relatively superior.

The corresponding drag characteristics for the airfoil are shown in Fig. 3. There is an almost linear rise in the drag coefficient (C_D) with α for all three cases. For the Joukowsky airfoil with splined cylinder (Fig. 3c), C_D remains quite small for $\alpha \leq 15$ deg. It attains a maximum value of around 2.5 at $\alpha = 50$ deg for the airfoil with a smooth or rough cylinder. On the other hand, maximum C_D is about 1.95 in the case of the splined cylinder. The lower drag coupled with a higher lift in case of the airfoil with a splined cylinder appears quite promising for practical aerodynamic applications. In Table 3, the slope $dC_D/d\alpha$ is listed for $U_C/U = 0$ and 4. Note, by application of the momentum injection, flow separation near the leading edge is avoided and the local pressure on the upper surface remains much lower compared to that at the lower surface of the airfoil. This results in a large normal force acting perpendicular to the airfoil. Because the drag of an airfoil is proportional to the sine component, i.e., $C_D \propto \sin \alpha$, of this normal force, it contributes more to C_D as α is increased. The rate of momentum injection increases the slope $dC_D/d\alpha$ in all three cases (Table 3).

The lift-to-drag ratio (C_L/C_D) for the airfoil with three different cylinder geometries is plotted in Fig. 4. The C_L/C_D has a peak in the range $0 \leq \alpha \leq 10$ deg, before stall. In the case

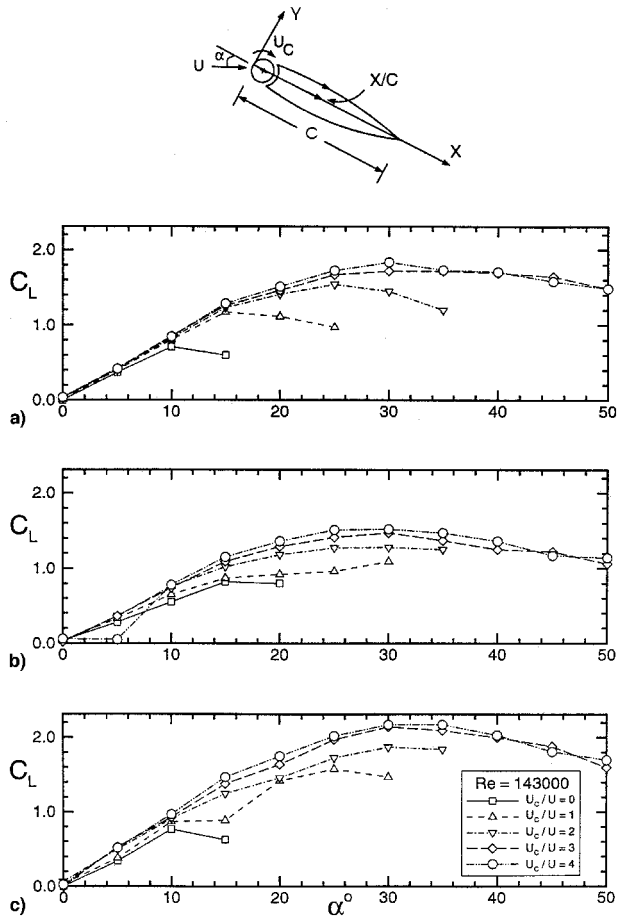

Fig. 2 Experimentally obtained lift coefficient for the Joukowski airfoil in presence of momentum injection: a) smooth leading-edge rotating cylinder, b) rough cylinder, and c) splined cylinder.

of splined cylinder, large values of C_L/C_D are achieved, resulting from a combination of high-lift and low-drag coefficients. Beyond stall, the C_L/C_D ratio drops off rapidly and there is only little momentum injection effect. At high angles of attack ($\alpha \geq 20$ deg), both the lift and the drag coefficients show an increase, keeping the C_L/C_D ratio low. Further appreciation in this regard can be obtained by examining C_L vs C_D plots for the three cases (Fig. 5). For the splined cylinder, the steep gradient of the plot suggests a favorable performance. In Fig. 6, variation of both C_L as well as C_L/C_D with α are plotted for the three cases. These results clearly establish significant changes brought about by the surface condition of a momentum-injecting rotating cylinder.

Results in Fig. 7 focus on the variation of C_L with α beyond the nominal stall angle of 10 deg (reference case), as affected by the surface roughness of the rotating element and U_C/U. For the smooth cylinder case, as expected, the lift coefficient first dips at stall followed by a monotonic rise with an increase in the angle of attack in the range tested ($\alpha \leq 50$ deg), in absence of the momentum injection. The effect of U_C/U is to delay the stall to around 30 deg for $U_C/U = 4$ with an increase in C_L by $\approx$ 160% as mentioned before. Now the discontinuity in the C_L vs α plot at the stall is eliminated. Note, the flat peak suggests the onset of a gradual stall, a desirable feature. The presence of the splined surface accentuates this behavior resulting in higher slope of the lift curve, increased $C_{L,max}$, and a slightly increased delay in the onset of stall ($\approx$32 deg), which continues to be gradual. The corresponding plots for the C_D variation are presented in Fig. 8. The relatively small increase in the drag for the splined cylinder case suggests effectiveness of the MSBC even at moderately high angles of attack. At an angle of attack of 30 deg, a reduction in the drag coefficient

Table 1 Comparative performance of the three rotating cylinders in terms of the maximum lift coefficient and the stall angle for $U_C/U = 3$ and 4

	$U_C/U = 0$		$U_C/U = 3, 4$	
Cylinder	α_{stall}, deg	$C_{L,max}$	α_{stall}, deg	$C_{L,max}$
Smooth	10	0.70	35	1.75
Rough	15	0.80	30	1.50
Splined	10	0.75	35	2.15

Table 2 Average values of $dC_L/d\alpha$ for three rotating cylinders

Range of α, deg	Smooth cylinder	Rough cylinder	Splined cylinder
0–20	4.30	3.87	5.01
0–30	3.44	2.87	4.11
30–50	−0.86	−1.15	−1.29

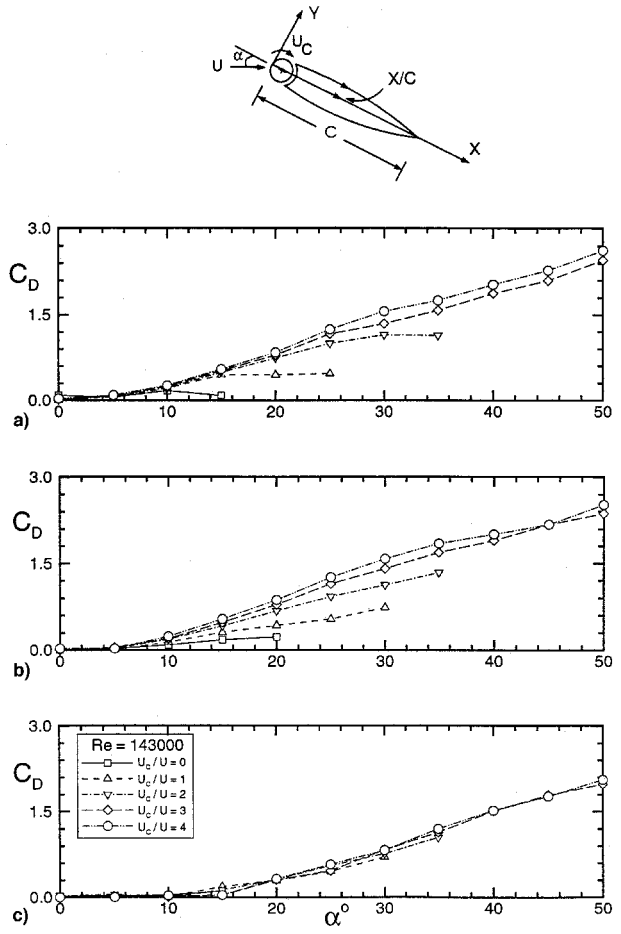

Fig. 3 Experimentally obtained drag coefficient for the Joukowski airfoil in presence of momentum injection: a) smooth leading-edge rotating cylinder, b) rough cylinder, and c) splined cylinder.

from $C_D \approx 1.6$ for the smooth cylinder case in the absence of momentum injection to $C_D \approx 0.7$ for the airfoil with a splined cylinder at $U_C/U = 2$ is indeed impressive. It amounts to a 56% reduction in the drag coefficient.

Pressure Distribution

Extensive wind-tunnel tests provided a wealth of information in terms of the pressure distribution with respect to different flow parameters. Some typical results for the smooth and splined surface cylinders are presented in Fig. 9 to explain

Table 3 Average values of $dC_D/d\alpha$ as affected by the cylinder surface condition and rate of momentum injection

Cylinder	$U_C/U = 0$ ($0 \le \alpha \le 10$ deg)	$U_C/U = 4$ ($0 \le \alpha \le 50$ deg)
Smooth	0.997	2.865
Rough	0.229	2.865
Splined	0.516	2.292

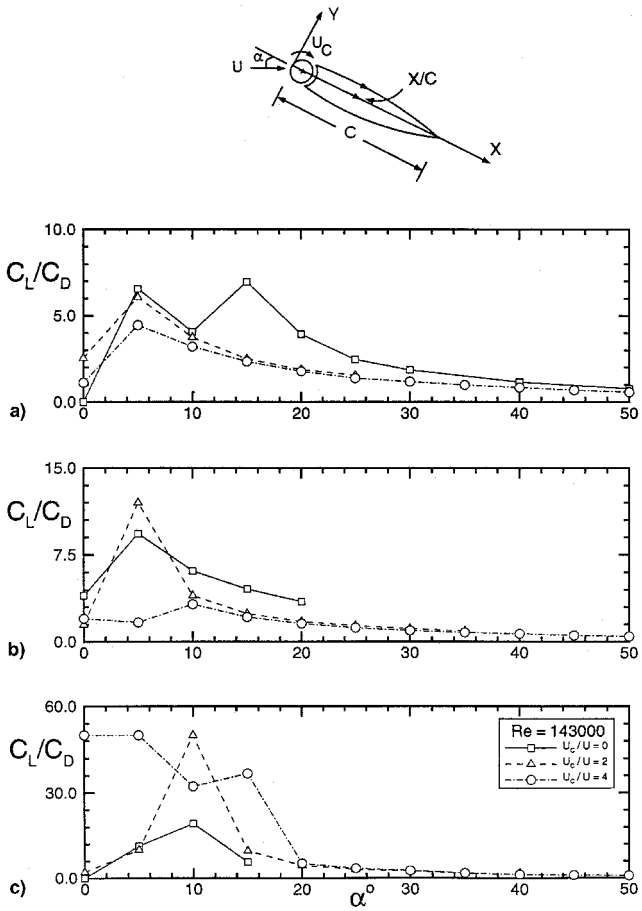

Fig. 4 Experimentally obtained lift/drag ratio of the Joukowski airfoil in presence of momentum injection: a) smooth cylinder, b) rough cylinder, and c) splined cylinder.

the physical effects of momentum injection on the flow past the airfoil. As mentioned earlier, the airfoil is symmetric about its chord and, hence, has similar pressure distribution on the top and bottom surfaces resulting in a zero lift at $\alpha = 0$. At $\alpha = 5$ deg (Fig. 9a), the pressure on the top surface of the airfoil is lower compared to that on the bottom surface. As α is increased farther, the pressure on the top surface becomes even lower (Fig. 9b). On the other hand, there is no change in the pressure distribution on the bottom surface. Also note the presence of a near-stagnation value ($C_P \approx 0.9$) at the bottom of the leading edge. The airfoil has not yet stalled at $\alpha = 10$ deg. Introduction of the momentum injection does not bring about any noticeable changes in the pressure distribution, as the flow is not separated. With a further increase in the angle of attack ($\alpha = 15$ deg), the airfoil stalls completely in the absence of the momentum injection ($U_C/U = 0$). As the momentum injection is increased from $U_C/U = 0$ to 4, the flow separation on the top surface is eliminated completely. The pressure coefficient C_P reaches a minimum value of -4.0 near the upper leading edge. A similar trend persists when α is further increased to 40 deg (Figs. 9d–9f). The peak negative C_P is about -6.0 at the top face of the rotating cylinder ($U_C/U = 4$), which

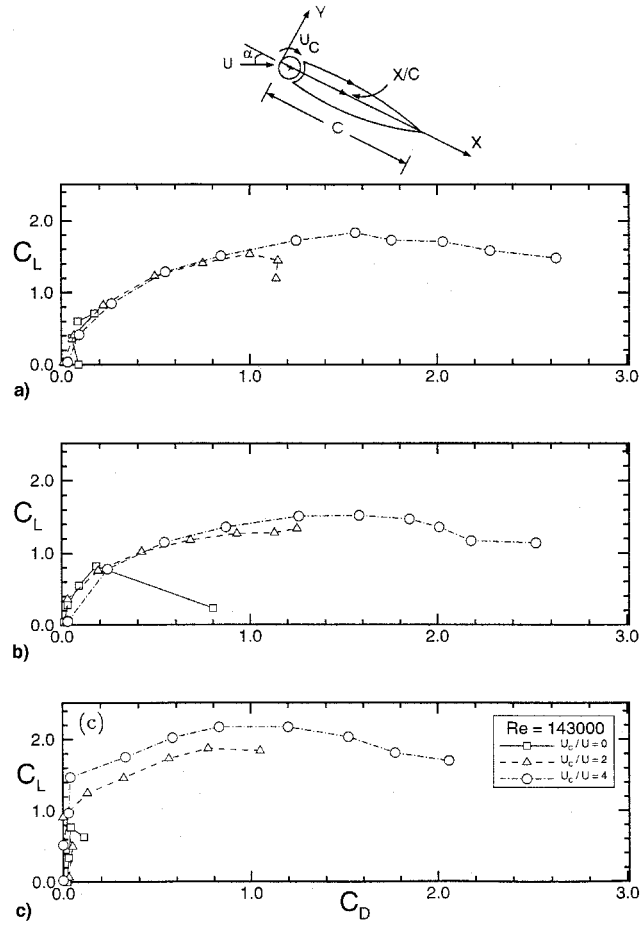

Fig. 5 Variation of C_L with C_D for the Joukowski airfoil in presence of momentum injection: a) smooth cylinder, b) rough cylinder, and c) splined cylinder.

significantly contributes to a large increase in the lift. As expected, in presence of the momentum injection, the point of separation on the top surface moves toward the trailing edge with an increase in the cylinder rotation.

Numerical Simulation

Panel Method

The precise numerical solution of this complex problem involving moving boundaries can be obtained by solving the general time-dependent Navier–Stokes equations incorporating a suitable turbulence model. The relatively simpler case of a cylinder (in the absence of an airfoil) subjected to a time-dependent rate of rotation in a uniform stream was investigated by Ou.[21] Only numerical simulation results at a very low Reynolds number ($Re = 2 \times 10^2$) were presented, which has little relevance to real-life flow problems. Hassan and Sankar[22] modeled compressible flow past an airfoil with leading-edge rotating cylinder using the full Reynolds-averaged Navier–Stokes equations with body-fitted curvilinear grid and an implicit finite difference scheme. However, for realistic values of the Reynolds number, this would demand significant computational effort and cost. On the other hand, judicious modeling of the flow character can provide information of sufficient accuracy for all engineering design purposes with nominal computational tools and insignificant cost. To that end an extension of the well-developed panel code to multielement systems with momentum injection appeared quite attractive.

During the past three decades, the classical panel method involving the distribution of surface-singularities has evolved to a sophisticated level where it can tackle complex geometries and a flow separation condition.[23–25] Maskew and Dvorak[23]

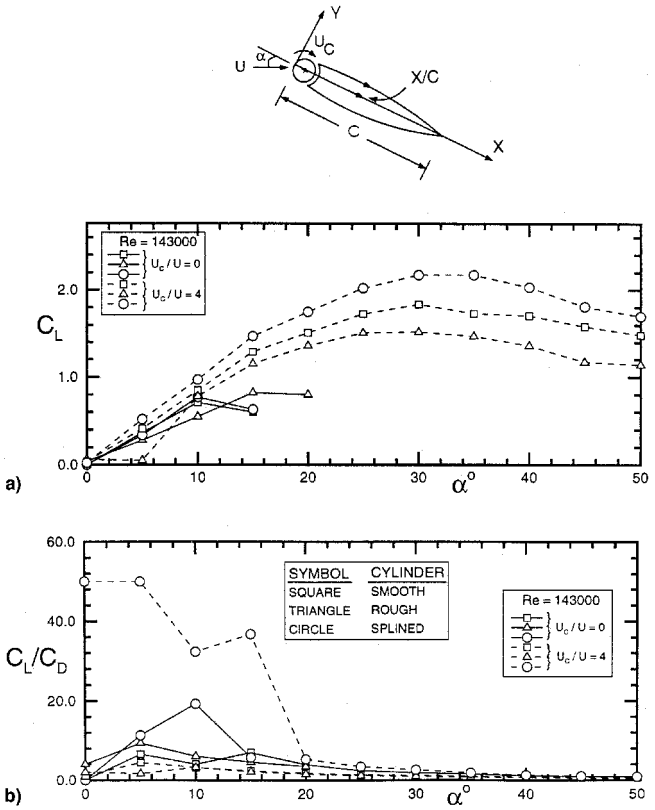

Fig. 6 Comparative study showing the effect of cylinder surface and momentum injection on the variation of a) C_L with α and b) C_L/C_D with α.

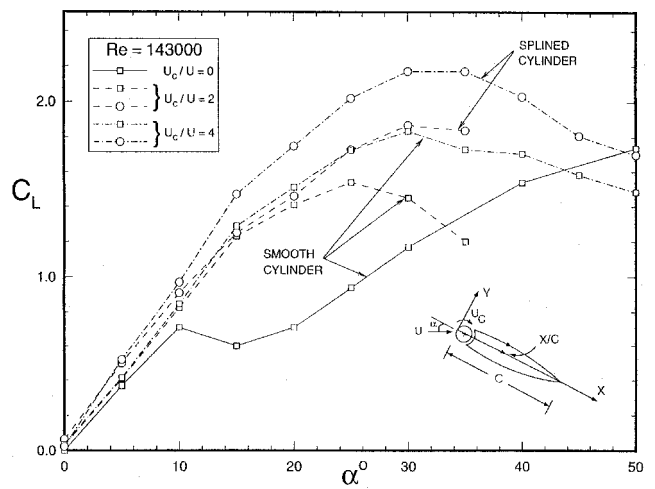

Fig. 7 Comparative study showing the effect of surface roughness and momentum injection on the lift coefficient at high angles of attack.

modeled separated flow by free-vortex lines having a known constant vorticity but initially of an unknown shape. Successive iterations yield the converged wake shape. Ribaut[24] accounted for the vorticity dispersion through dissipation and diffusion leading to a finite wake. The first-order panel method employing linearly varying vorticity along each panel and incorporating dispersion in the wake to model the separated flow[25] is also attractive.

In the present study the airfoil with the momentum injecting rotating cylinder is represented by a large number of panels (100–150). Each panel has a continuous distribution of linearly varying vorticity and a constant source strength (Fig. 10). In the attached flow model, the flow does not separate from

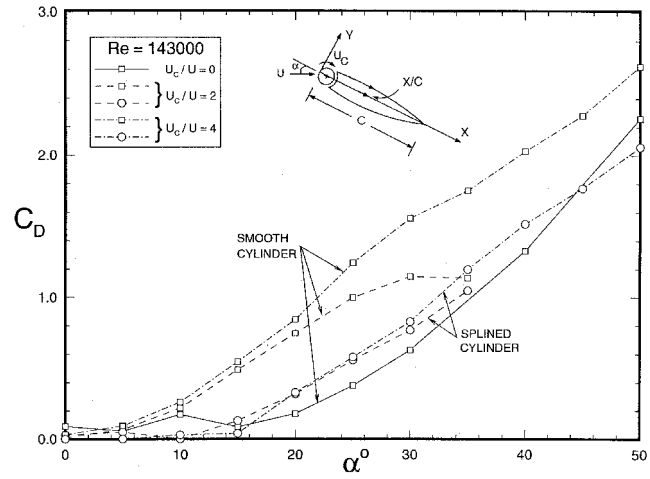

Fig. 8 Effect of momentum injection with the splined surface cylinder on the variation of C_D with α. The smooth cylinder results are also presented to serve as a reference.

the airfoil, whereas in the separated flow model, the separation is modeled by the free-vortex lines emanating from the lower and upper separation points on the airfoil. The lower separation point coincides with the trailing edge of the airfoil. The free-vortex lines are also discretized into panels. At the beginning of the free-vortex line, the vorticity strength is taken to be equal to that at the separation point. The vorticity is allowed to dissipate at a given rate along the free-vortex lines resulting in a finite wake. An iterative scheme leads to the final solution. In the single-element model the airfoil and the rotating cylinder are treated as a single physical object. Whereas, in the two-element model, the airfoil and the rotating cylinder are descretized as distinct bodies. Further details of the numerical modeling are given by Munshi.[26]

Pressure Distribution

Figure 11 compares pressure distribution plots on the surface of the airfoil obtained through the numerical scheme and wind-tunnel tests. The experimental data pertain to the case of the Joukowsky airfoil with a smooth cylinder. The numerical results were obtained using the two-element panel configuration as described earlier.

At α = 5 deg and in absence of momentum injection ($U_C/U = 0$), there is a good agreement between the theory and experimental data (Fig. 11a). However, at a higher rate of momentum injection ($U_C/U = 4$), the numerical scheme somewhat overpredicts the negative pressure on the top surface of the airfoil. On the other hand, presence of a large suction peak at the rotating cylinder is successfully captured by the numerical scheme. Because of the limited number of pressure taps on the surface of the rotating cylinder, the suction peak could be captured only partially during the experiment; though a tendency toward large negative C_P is evident. Overall, there is a satisfactory agreement between the numerical and experimental pressure distribution plots over the complete airfoil. An increase in α to 10 deg (Fig. 11b) makes the suction peak even more pronounced. Close to the trailing edge the flow is almost separated at $U_C/U = 0$, indicating a tendency to stall. The complete stall at still higher angles of attack (α = 15 deg) is accurately captured by the numerical scheme. In the presence of momentum injection ($U_C/U = 4$), the point of separation is pushed further downstream ($X/C \approx 0.6$). The effect of the momentum injection diminishes as X/C increases and becomes negligible beyond $X/C \approx 0.6$, which is expected because of the vorticity dispersion and dissipation effects.

Comparative Studies

Figures 12–14 present comparison of results obtained using the numerical schemes and the wind-tunnel data. Numerically

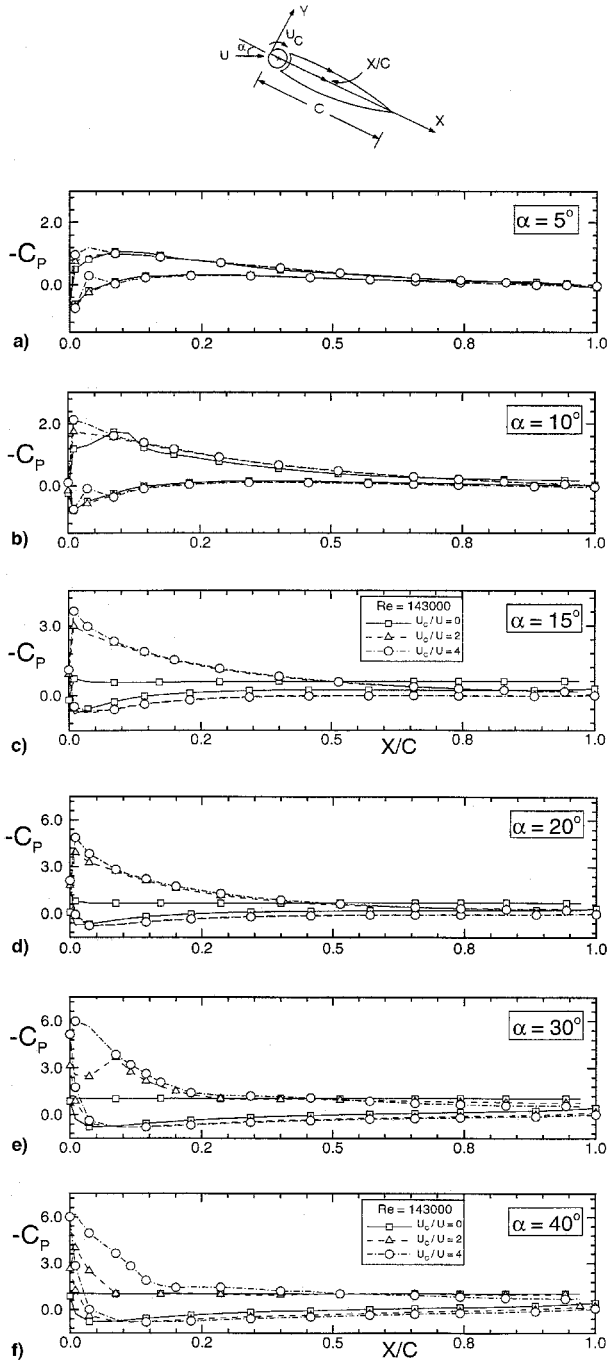

Fig. 9 Experimentally obtained pressure distribution for the Joukowski airfoil with the MSBC provided by a smooth surface cylinder. α = a) 5, b) 10, c) 15, d) 20, e) 30, and f) 40 deg.

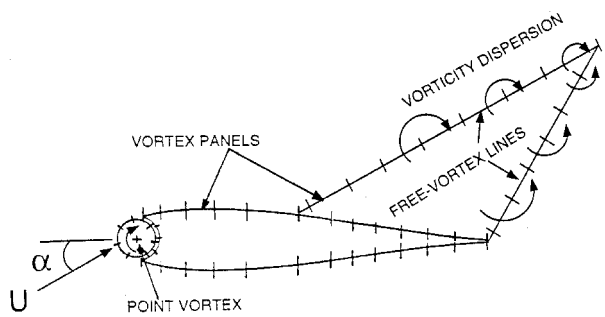

Fig. 10 Two-element panel configuration modeling the separated flow past a symmetrical Joukowski airfoil in presence of the MSBC.

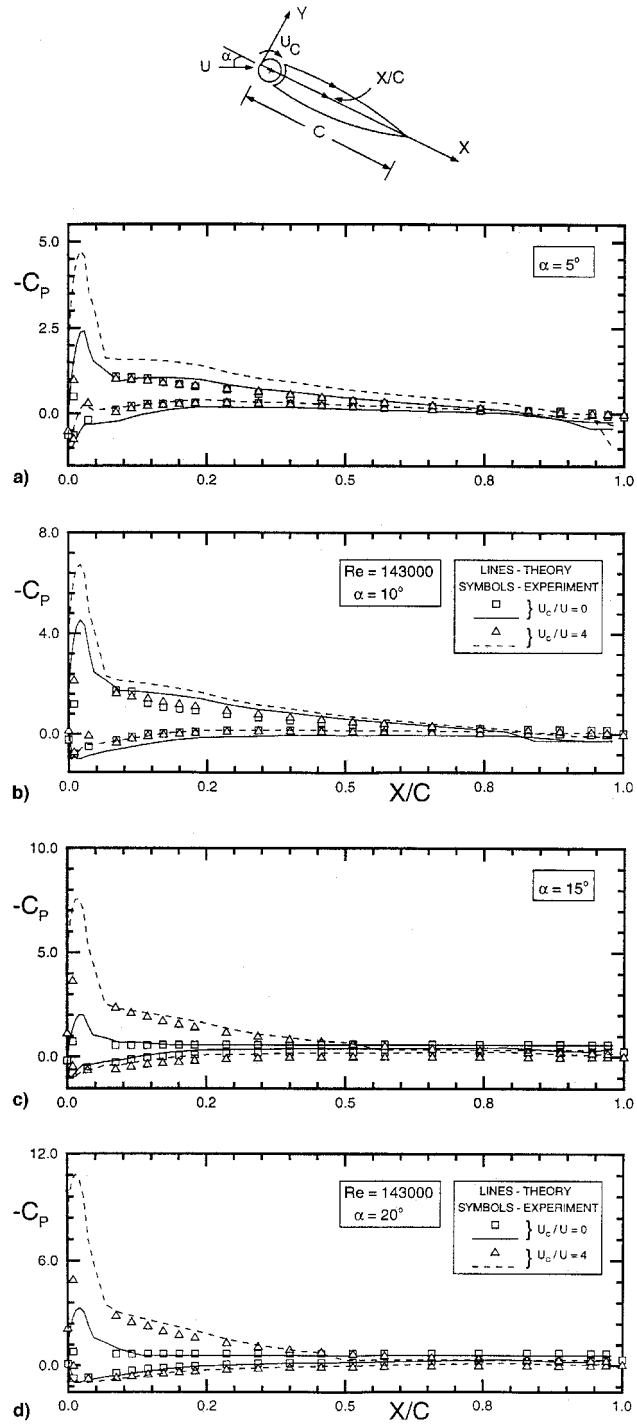

Fig. 11 Comparison of the numerically obtained pressure distribution with the experimental data for a Joukowski airfoil with the MSBC. α = a) 5, b) 10, c) 15, and d) 20 deg.

obtained pressure plots using a single- and two-element panel formulations with the attached flow model are shown in Fig. 12. The results are essentially similar except for the suction peak, which is larger for the two-element case. Fig. 13a shows a comparison between attached and separated flow solutions for the single-element configuration. As expected, the separated flow results agree better with the experimental data because they are more realistic. The suction peak near the leading edge diminishes because of the flow separation. The discrepancy near the trailing edge (Fig. 12) is also eliminated. In Fig. 13b, the results for the single-element airfoil are compared with those obtained using the two-element model. The predic-

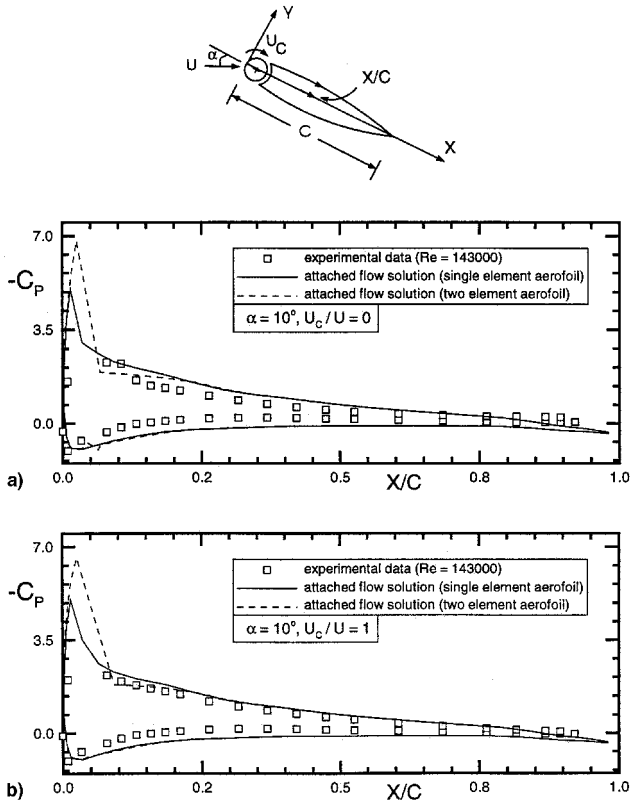

Fig. 12 Comparison between the results obtained through the single- and two-element numerical panel formulations in presence of the MSBC: a) α = 10 deg, U_C/U = 0; and b) α = 10 deg, U_C/U = 1. The experimental data are also included.

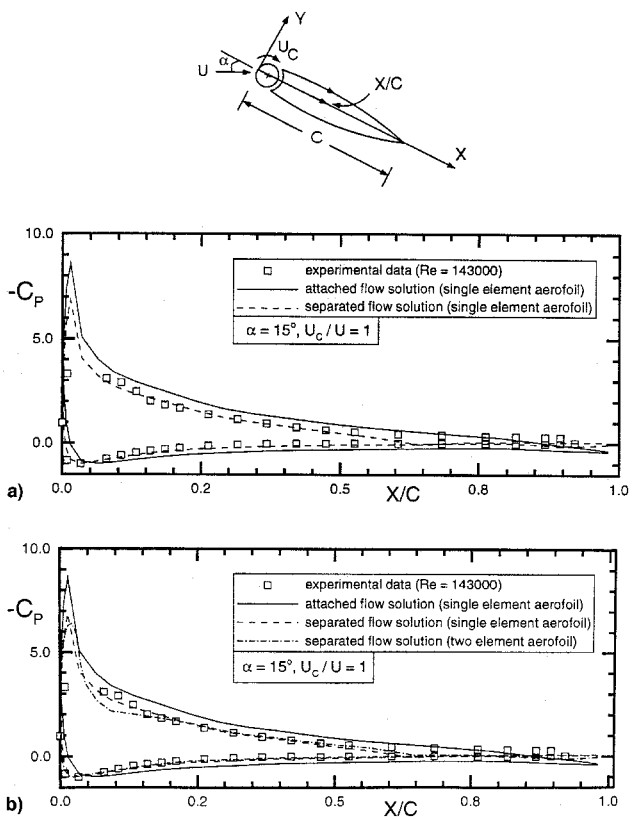

Fig. 13 Comparative studies of pressure plots in presence of the MSBC: a) attached vs separated flow solutions for a single-element formulation, and b) corresponding results for the two-element airfoil. The experimental data are also included.

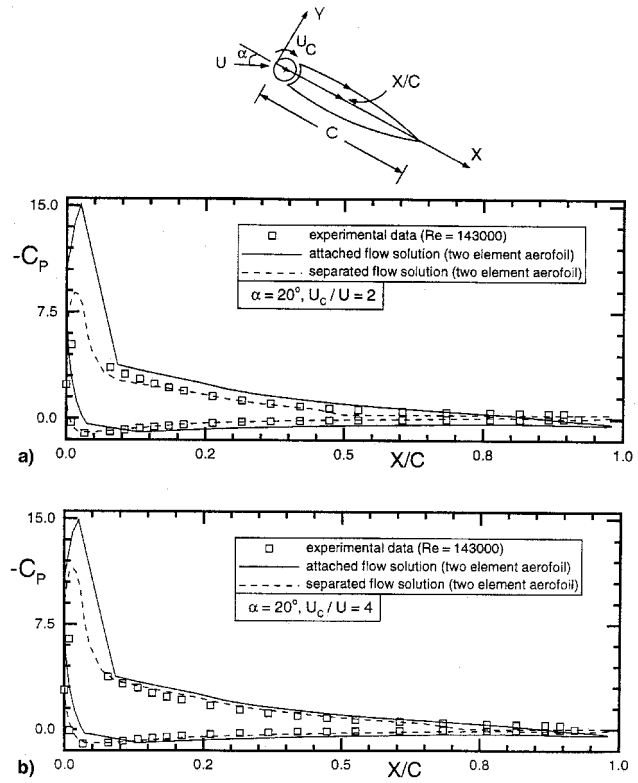

Fig. 14 Relative performance of the attached and separated flow models as applied to the two-element airfoil: a) α = 20 deg, U_C/U = 2; b) α = 20 deg, U_C/U = 4.

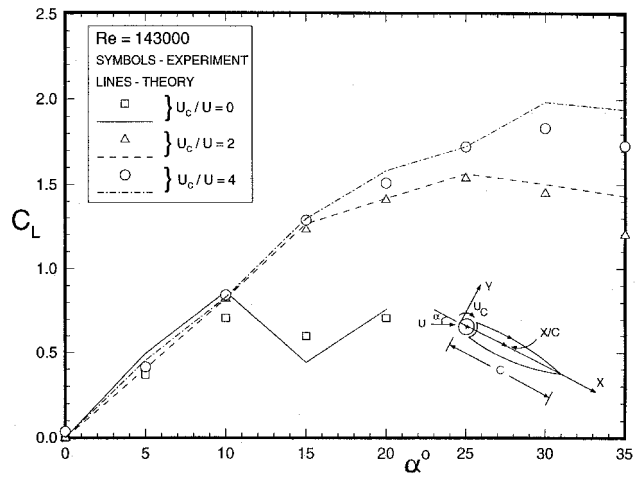

Fig. 15 Numerically obtained lift coefficient as compared to the experimental data for a Joukowski airfoil in presence of the MSBC.

tion by the two-element case shows a slight improvement. The spike in the suction peak (which is physically unlikely), is replaced by a smooth curve indicating a gradual change in the pressure. Figure 14 presents results at α = 20 deg for the two-element airfoil with attached and separated flow models. As can be expected, there is a significant improvement in prediction with the separated flow model. The unrealistically high suction peak predicted by the attached flow model is now substantially reduced. The modeling of flow separation near the leading edge agrees more closely with the actual physical process. The discrepancies between the numerical and experimental pressure values near the leading and the trailing edges are also eliminated.

Prediction of the Lift Coefficient

In Fig. 15, the numerically obtained lift coefficient is compared with that from the wind-tunnel tests. The C_L against the α curve agrees closely with the experimental results, particularly at low and moderate angles of attack ($\alpha \leq 20$ deg). The airfoil stall around $\alpha = 10$ deg is also captured by the numerical scheme accurately. However, for $\alpha \geq 30$ deg, the numerical results start to deviate from the experimental data. This can be expected as a result of relatively complex character of the flow. It indicates a need for improvement in the free vortex layer model of the wake at very high angles of attack.

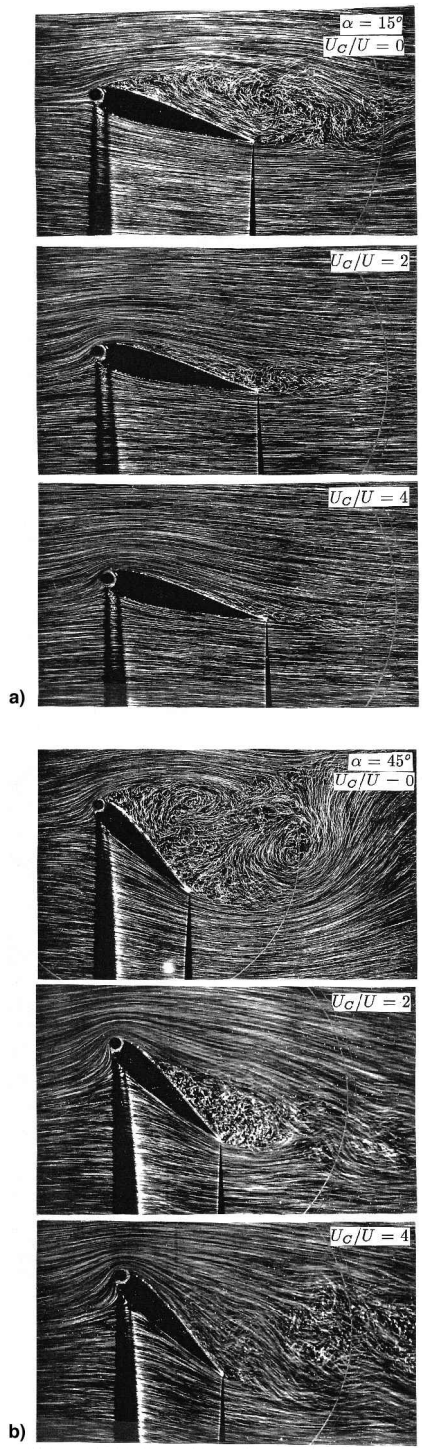

Fig. 16 Representative flow visualization pictures showing effectiveness of the boundary-layer control through momentum injection. The observed results compare well with the delay in separation predicted by the wind-tunnel test results and the panel code: α = a) 15 and b) 45 deg.

Flow Visualization

To get better appreciation as to the physical character of the complex flowfield as affected by the angle of attack and momentum injection parameters, an extensive flow visualization study was undertaken. It also gave useful information about the relative importance of the various parameters and, hence, assisted in planning of the experiments as well as the numerical analysis. The flow visualization tests were carried out in a closed-circuit water channel facility. The models were constructed from Plexiglas® and fitted with rotating cylinders driven by variable speed dc motors. A suspension of fine polyvinyl chloride powder was used in conjunction with slit lighting to visualize streaklines. Both angle of attack and cylinder speed were systematically changed and still photographs as well as video movies taken.

The study showed, rather dramatically, effectiveness of this form of boundary-layer control (Fig. 16). For the leading-edge smooth cylinder at $\alpha = 15$ deg ($Re = 2.94 \times 10^4$) and in absence of the cylinder rotation, a well-defined early separation, almost at the leading edge, results in a wide wake with large-scale vortices sweeping away downstream (Fig. 16a). As the momentum injection is increased to $U_C/U = 1$, there is flow reattachment of the separated shear layer at about $X/C \approx 0.6$ forming a large bubble with recirculating flow. However, the momentum injection is not sufficient to keep the flow attached and it separates again rather quickly, forming a well-organized wake. Compared to the case of $U_C/U = 0$, the streamlines move closer on the upper surface of the airfoil, diminishing the wake width considerably ($\approx 0.48C$). At $U_C/U = 2$, the streamlines are very close to the upper surface and the wake is quite small ($\approx 0.3C$). The separation bubble has disappeared completely. Note the presence of a stagnation point near the leading edge on the bottom surface of the airfoil. The separation point is further pushed toward the trailing edge. At $U_C/U = 4$, an essentially attached flow is established over most of the upper surface of the airfoil, even at such a high angle of attack, considerably beyond the nominal stall angle of around 10 deg. Similar trends persist even at $\alpha = 45$ deg (Fig. 16b).

The flow pattern in the wake of the airfoil was found to be quite unsteady with the vortex layer separating and forming a bubble on reattachment, the whole structure drifting downstream, diffusing, and regrouping at different scales of vortices. Ultimately the flow sheds large as well as small vortices. This unsteady character of the separating shear layer and the wake is clearly evident in the flow visualization video. Thus the flow character indicated by the experimentally obtained time-averaged plots appear to be a fair description of the process.

Concluding Remarks

Based on the wind-tunnel, numerical, and flow visualization results, the following comments can be made:

1) Significant improvement in the lift coefficient as well as the delay in the stall angle could be achieved by judiciously selecting the rate of the momentum injection and cylinder surface geometry.

2) A momentum injection ratio of $U_C/U = 4$ indicates a practical limit to the beneficial effect of the momentum injection in increasing the lift. A further increase in the momentum injection is not likely to provide higher lift, but may affect the drag adversely.

3) Among the three different surface roughness conditions studied, the cylinder with axial splines was found to be the most effective. A 210% increase in the lift coefficient was achieved in this case.

4) In presence of the MSBC the stall becomes gradual and could be delayed to 50 deg.

5) The numerical scheme provides good approximation of the actual fluid dynamics of the MSBC as applied to a multielement airfoil at high angles of attack.

6) The flow visualization results dramatically confirm effectiveness of the MSBC in delaying separation.

Acknowledgment

This investigation was supported by the Natural Sciences and Engineering Research Council of Canada, Grant A-2181.

References

[1]Erickson, G. E., "High Angle-of-Attack Aerodynamics," *Annual Review of Fluid Mechanics*, Vol. 27, 1995, pp. 45–88.

[2]Goldstein, S., *Modern Developments in Fluid Mechanics*, Vols. 1 and 2, Oxford Univ. Press, Oxford, England, UK, 1938.

[3]Lachmann, G. V., *Boundary-Layer and Flow Control, Its Principles and Application*, Vol. 1, Pergamon, New York, 1961, pp. 1, 2.

[4]Rosenhead, L., *Laminar Boundary Layers*, Clarendon, Oxford, England, UK, 1966, pp. 111, 332–335, 547.

[5]Schlichting, H., *Boundary Layer Theory*, McGraw–Hill, New York, 1968, pp. 362–390.

[6]Chang, P. K., *Control of Flow Separation*, McGraw–Hill, New York, 1970, pp. 154–177.

[7]Gad-el-Hak, M., "Flow Control," *Applied Mechanics Review*, Vol. 42, No. 10, 1989, pp. 261–293.

[8]Wu, J. M., and Wu, J. Z., "Vortex Lift at a Very High Angle of Attack with Massively Separated Unsteady Flow," *Fluid Dynamics of High Angle of Attack*, edited by R. Kawamura and Y. Aihara, Springer–Verlag, Berlin, 1993, pp. 49–63.

[9]Modi, V. J., Mokhtarian, F., Fernando, M. S. U. K., and Yokomizo, T., "Moving Surface Boundary-Layer Control as Applied to Two-Dimensional Airfoils," *Journal of Aircraft*, Vol. 28, No. 2, 1991, pp. 104–112.

[10]Modi, V. J., Fernando, M. S. U. K., and Yokomizo, T., "Moving Surface Boundary-Layer Control: Studies with Bluff Bodies and Application," *AIAA Journal*, Vol. 29, No. 9, 1991, pp. 1400–1406.

[11]Modi, V. J., Shih, E., Ying, B., and Yokomizo, T., "Drag Reduction of Bluff Bodies Through Momentum Injection," *Journal of Aircraft*, Vol. 29, No. 3, 1992, pp. 429–436.

[12]Munshi, S. R., Modi, V. J., and Yokomizo, T., "Drag Reduction and Vibration Suppression of a D-Section Structural Member Through Momentum Injection," *International Journal of Offshore and Polar Engineering*, Vol. 5, No. 3, 1995, pp. 161–165.

[13]*Aviation Week and Space Technology*, Vol. 95, No. 16, Oct. 18, 1971, p. 19.

[14]*Aviation Week and Space Technology*, Vol. 95, No. 24, Dec. 13, 1971, Front Cover, p. 7.

[15]Wygnanski, I. J., and Seifert, A., "The Control of Separation by Periodic Oscillations," AIAA Paper 94-2608, June 1994.

[16]Chang, P. K., *Control of Flow Separation*, McGraw–Hill, New York, 1970, p. 302.

[17]*Jane's All the World Aircraft*, Samson Low, London, 1971–72, pp. 363–364.

[18]Cichy, D. R., Harris, J. W., and MacKay, J. K., "Flight Tests of a Rotating Cylinder Flap on a North American Rockwell, YOV-10A Aircraft," NASA CR-2135, Nov. 1972.

[19]Brown, D. A., "Peruvians Study Rotating-Cylinder Flap," *Aviation Week and Space Technology*, Vol. 88, No. 23, Dec. 1964, pp. 70–76.

[20]Modi, V. J., Ying, B., and Yokomizo, T., "An Approach to Design of the Next Generation of Fuel Efficient Trucks Through Aerodynamic Drag Reduction," *Proceedings of the ASME Winter Annual Meeting, Atlanta, USA*, edited by S. A. Velinsky, R. H. Fries, and D. Wang, DE-Vol. 40, American Society of Mechanical Engineers, New York, Nov. 1991, pp. 465–482.

[21]Ou, Y. R., "Mathematical Modeling and Numerical Simulation in External Flow Control," *Flow Control*, edited by M. D. Gunzburger, Springer–Verlag, New York, 1995, pp. 219–255.

[22]Hassan, A. A., and Sankar, L. N., "Separation Control Using Moving Surface Effects: A Numerical Simulation," *Journal of Aircraft*, Vol. 29, No. 1, 1992, pp. 131–139.

[23]Maskew, B., and Dvorak, F. A., "The Prediction of $C_{L,\max}$ using a Separated Flow Model," *Journal of the American Helicopter Society*, Vol. 23, April 1978, pp. 2–8.

[24]Ribaut, M., "A Vortex Sheet Method for Calculating Separated Two-Dimensional Flows," *AIAA Journal*, Vol. 21, No. 8, 1983, pp. 1079–1084.

[25]Mukherjea, S., and Bandyopadhyay, G., "Separated Flow about a Wedge," *The Aeronautical Journal of the Royal Aeronautical Society*, Vol. 94, June–July 1990, pp. 196–202.

[26]Munshi, S. R., "Aerodynamics and Dynamics of Bluff Bodies in Presence of the Moving Surface Boundary-Layer Control," Ph.D. Dissertation, Dept. of Mechanical Engineering, Univ. of British Columbia, Vancouver, BC, Canada, Jan. 1996, pp. 66–81.